Compound simulation of fluvial floods and storm surges in a global coupled river-coast flood model

Model development and its application to 2007 Cyclone Sidr in Bangladesh

Ikeuchi, Hiroaki; Hirabayashi, Yukiko ; Yamazaki, Dai; Muis, S.; Ward, Philip J.; Winsemius, Hessel; Verlaan, Martin; Kanae, Shinjiro

DOI
10.1002/2017MS000943

Publication date
2017

Document Version
Final published version

Published in
Journal of Advances in Modeling Earth Systems

Citation (APA)
Ikeuchi, H., Hirabayashi, Y., Yamazaki, D., Muis, S., Ward, P. J., Winsemius, H., Verlaan, M., & Kanae, S. (2017). Compound simulation of fluvial floods and storm surges in a global coupled river-coast flood model: Model development and its application to 2007 Cyclone Sidr in Bangladesh. *Journal of Advances in Modeling Earth Systems*, *9*(4), 1847-1862. https://doi.org/10.1002/2017MS000943

AGU PUBLICATIONS

Journal of Advances in Modeling Earth Systems

RESEARCH ARTICLE
10.1002/2017MS000943

Key Points:
- Development of a first global coupled river-coast flood model that facilitates compound simulation of fluvial flood and storm surge
- Incorporation of sea level dynamics into river routing enhanced model performance in reproducing river water levels
- The coupled model was applied to Cyclone Sidr, demonstrating cyclonic storm surge propagation through rivers

Correspondence to:
H. Ikeuchi,
ikeuchi@rainbow.iis.u-tokyo.ac.jp

Citation:
Ikeuchi, H., Y. Hirabayashi, D. Yamazaki, S. Muis, P. J. Ward, H. C. Winsemius, M. Verlaan, and S. Kanae (2017), Compound simulation of fluvial floods and storm surges in a global coupled river-coast flood model: Model development and its application to 2007 Cyclone Sidr in Bangladesh, *J. Adv. Model. Earth Syst.*, *9*, 1847–1862, doi:10.1002/2017MS000943.

Received 13 FEB 2017
Accepted 3 JUL 2017
Accepted article online 13 JUL 2017
Published online 8 AUG 2017

Compound simulation of fluvial floods and storm surges in a global coupled river-coast flood model: Model development and its application to 2007 Cyclone Sidr in Bangladesh

Hiroaki Ikeuchi[1,2,3], Yukiko Hirabayashi[2], Dai Yamazaki[2,4], Sanne Muis[3], Philip J. Ward[3], Hessel C. Winsemius[3,5], Martin Verlaan[5,6], and Shinjiro Kanae[7]

[1]Department of Civil Engineering, The University of Tokyo, Tokyo, Japan, [2]Institute of Industrial Science, The University of Tokyo, Tokyo, Japan, [3]Institute for Environmental Studies (IVM), Vrije Universiteit Amsterdam, Amsterdam, The Netherlands, [4]Department of Integrated Climate Change Projection Research, Japan Agency for Marine-Earth Science and Technology, Yokohama, Japan, [5]Deltares, Delft, The Netherlands, [6]Department of Applied Mathematics, Delft University of Technology, Delft, The Netherlands, [7]Department of Civil and Environmental Engineering, Tokyo Institute of Technology, Tokyo, Japan

Abstract Water-related disasters, such as fluvial floods and cyclonic storm surges, are a major concern in the world's mega-delta regions. Furthermore, the simultaneous occurrence of extreme discharges from rivers and storm surges could exacerbate flood risk, compared to when they occur separately. Hence, it is of great importance to assess the compound risks of fluvial and coastal floods at a large scale, including mega-deltas. However, most studies on compound fluvial and coastal flooding have been limited to relatively small scales, and global-scale or large-scale studies have not yet addressed both of them. The objectives of this study are twofold: to develop a global coupled river-coast flood model; and to conduct a simulation of compound fluvial flooding and storm surges in Asian mega-delta regions. A state-of-the-art global river routing model was modified to represent the influence of dynamic sea surface levels on river discharges and water levels. We conducted the experiments by coupling a river model with a global tide and surge reanalysis data set. Results show that water levels in deltas and estuaries are greatly affected by the interaction between river discharge, ocean tides and storm surges. The effects of storm surges on fluvial flooding are further examined from a regional perspective, focusing on the case of Cyclone Sidr in the Ganges-Brahmaputra-Meghna Delta in 2007. Modeled results demonstrate that a >3 m storm surge propagated more than 200 km inland along rivers. We show that the performance of global river routing models can be improved by including sea level dynamics.

1. Introduction

The world's mega-delta regions are highly sensitive to multiple risks from water-related disasters, such as fluvial flooding due to overbank flows from rivers and coastal storm surges caused by cyclones and hurricanes [*Wong et al.*, 2014]. Since deltas are inhabited by more than 500 million people worldwide [*Syvitski and Saito*, 2007], the potential impacts of floods in these regions are of great concern. In particular, mega-deltas in Southeast Asia, such as the Ganges-Brahmaputra-Meghna (GBM) Delta, are prone to both river and coastal flooding due to heavy and intensive monsoon rainfall and storm surges caused by cyclones [*Syvitski et al.*, 2009]. Climate change could additionally augment flood risks in these regions. Future projections suggest that the frequency of fluvial floods will increase in large parts of the world, particularly in Asian and African regions, due to increases in extreme discharges [*Cisneros et al.*, 2014; *Hirabayashi et al.*, 2013; *Winsemius et al.*, 2016]. Furthermore, recent studies indicate that some coastal regions can expect more intense storm surges [*Androulidakis et al.*, 2015; *Lin and Emanuel*, 2016; *Vousdoukas et al.*, 2016]. When river and coastal floods occur at the same time or in quick succession, their impacts could be more devastating than when either occurs separately [*Kew et al.*, 2013; *Klerk et al.*, 2015; *Wahl et al.*, 2015]. The need to improve our understanding of compound hazards has been recognized by the research community as well as the user community of natural hazards information [e.g., *Seneviratne et al.*, 2012; *Leonard et al.*, 2014]. Thus, it is of great importance to have an understanding of how these compound fluvial and coastal floods affect mega-delta regions. Since such risks are common to most mega-delta regions, continental-scale, or global-scale models can be used to assess their influence at the large scale.

In recent years, large-scale assessments of fluvial flooding have been improved through flood frequency analysis [*Milly et al*., 2002; *Hirabayashi et al*., 2008; *Dankers et al*., 2014; *Trigg et al*., 2016]; and the assessment of exposed populations [*Hirabayashi et al*., 2013; *Jongman et al*., 2012a] and flood damages [*Jongman et al*., 2012b; *Ward et al*., 2013, 2014; *Winsemius et al*., 2016]. These assessments have been facilitated through the development of continental-scale or global-scale river routing models (e.g., PCR-GLOBWB-Dynrout, *Winsemius et al*. [2013]; LISFLOOD-FP *Van Der Knijff et al*. [2010]). However, their application to the analysis of compound fluvial flooding and coastal storm surges remains limited primarily due to the lack of representation of backwater effects in river discharge calculations and the lack of global coastal water level data. The backwater effect is a phenomenon where changes in water levels downstream are propagated upstream. Storm surges cause extreme sea levels at river mouths, which may propagate through rivers upstream by backwater effects. While the backwater effect is expressed as a varying water level in river discharge calculations, most global river routing models use a kinematic wave equation, thereby neglecting the backwater effect within rivers in hydraulic calculations. This means that the simultaneous assessment of fluvial flooding and storm surges has not yet been achieved at the continental-scale to global-scale.

Recently, there has been growing attention to the need to model the interaction of fluvial flooding and coastal surges [*Hoitink and Jay*, 2016; *Ward et al*., 2015]. Several studies have been carried out using two-dimensional or three-dimensional hydrodynamic models at basin-scales or regional-scales, for example, in Bangladesh [*Karim and Mimura*, 2008], Taiwan [*Chen and Liu*, 2014], and the United Kingdom [*Skinner et al*., 2015]. However, their high-computational loads limit their application to relatively small-scale analyses, precluding basin-scale, continental-scale, and global-scale assessments of compound fluvial and coastal flooding. Studies on coastal storm surges have also been expanded in recent years, for example, to encompass flood losses in the world's coastal cities [*Hallegatte et al*., 2013; *Hinkel et al*., 2014]. *Muis et al*. [2016] developed the first global-scale reanalysis data set of tide and surge water levels based on hydrodynamic modeling, the Global Tide and Surge Reanalysis (GTSR) data set [*Muis et al*., 2016]. However, these studies only analyzed extreme water levels along the coast and their effect of flooding on land, and did not investigate propagation effects through rivers.

In this paper, we address several of the issues outlined above; the objectives of this study are twofold: (1) to develop a global coupled river-coast flood model; and (2) to conduct a simulation to assess the impact of compound fluvial flooding and storm surges on water levels in Asian mega-delta regions. To achieve this, we advance our physically based approach of large-scale fluvial flood modeling, by integrating a global river routing model with GTSR. The current state-of-the-art improvements are briefly explained below. *Ikeuchi et al*. [2015] first estimated the effect of sea level rise (SLR; values projected at the end of the 21st century) on fluvial flood inundation in the GBM Delta employing a global river routing model. They found that SLRs of 1 m and 2 m would exacerbate fluvial floods, increasing inundation depths over wide areas. However, they ignored spatiotemporal variation in sea levels caused by storm surges, which can cause much higher water level changes (e.g., $>$6 m) than SLR. In this paper, we bring these advances in river and storm surge modeling together, and develop a framework for the simultaneous modeling of fluvial floods and coastal storm surges applicable to global-scale analyses. Beyond model development at a global-scale, we analyze the performance of the model in reproducing water levels regionally, using the Cyclone Sidr event in the Bay of Bengal in 2007 as a case study. We analyze the effects of coastal water levels and river flows on inundation within the delta. Quantifying the impacts of coastal flooding on river flood inundation, this study will be a basis to provide better information for flood risk management in mega-delta regions.

2. Methods

Here we provide an overview of the method, followed by detailed descriptions of each model and the coupling scheme. We used a global river routing model, Catchment-based Macro-scale Floodplain model (CaMa-Flood, ver. 3.6.2) [*Yamazaki et al*., 2011], and a global reanalysis of tide and surge water levels, the Global Tide and Surge Reanalysis (GTSR) data set [*Muis et al*., 2016]. The coupling scheme was introduced into CaMa-Flood to deal with changing sea surface levels calculated by GTSR.

2.1. Global River Routing Model: CaMa-Flood

The global river routing model, CaMa-Flood, integrates runoff calculated from a land surface model along a prescribed river network map to obtain river discharge, flood inundation area, and depth information. The

river network map was delineated from SRTM3 Digital Elevation Model (DEM) [*Farr et al*., 2007] and a high-resolution flow direction map, HydroSHEDS [*Lehner et al*., 2008]. The original resolution of these data sets is 90 m, and a coarser river network is derived from them for use in the CaMa-Flood river model to reduce computational costs [*Yamazaki et al*., 2009]. The spatial resolution of CaMa-Flood can easily be modified to any resolution coarser than 90 m [*Yamazaki et al*., 2011], and river basins are discretized at that resolution into calculation units (called unit-catchments), which are consisted of subgrid river and floodplain topography (shown as Figure 1 in *Yamazaki et al*. [2011]).

Implementation of a one-dimensional flow equation (a local inertial equation) [*Bates et al*., 2010; *Yamazaki et al*., 2013] has facilitated global-scale flood risk analysis [*Hirabayashi et al*., 2013] with high-computational efficiency. Due to the use of a local inertial equation, the simulation of flood inundation including SLR impacts has been achieved [*Ikeuchi et al*., 2015]. The local inertial equation is discretized using a forward in time finite difference method as follows:

$$Q^{t+\Delta t} = \frac{Q^t - gAS\Delta t}{\left(1 + \frac{gn^2|Q^t|\Delta t}{Ah^{4/3}}\right)} \tag{1}$$

where Q^t and $Q^{t+\Delta t}$ are the discharges (m^3/s) at the time t and $t + \Delta t$, respectively, g is the gravitational acceleration (m/s^2), A is the flow cross-sectional area (m^2), S is the water surface slope, n is the Manning's roughness coefficient ($m^{-1/3}$ s), and h is the water depth (m). The Manning coefficient was set as 0.03 for river channels, which is the default value used for the CaMa-Flood model [*Yamazaki et al*., 2011] based on *Chow* [1959]. The discharge and the water storage are prognostic variables at each calculation time step, followed by determination of diagnostic variables such as water level, inundation area, and depth. The water storage at each grid cell is calculated by a continuity equation as follows:

$$S_i^{t+\Delta t} = S_i^t + \sum_k^{upstream} Q_k^t \Delta t - Q_i^t + A_{ci} R_i^t \Delta t \tag{2}$$

where $S_i^{t+\Delta t}$ and S_i^t are total water storage (m^3) at the time step $t + \Delta t$ and t, Q_i^t is the discharge (m^3/s) at the time step t, A_{ci} is the unit-catchment area (m^2), R_i^t is the runoff forcing (mm/s) at the time step t at the grid i.

CaMa-Flood has two parameters of river channel cross sections, i.e., river channel width and height. The river channel width is determined either from the Global Width Database for Large Rivers (GWD-LR, *Yamazaki et al*.[2014b]) or by an empirical equation as follows:

$$W = \max[0.40 \times R_{up}^{0.75}, 10.0] \tag{3}$$

where W is the river channel width (m) and R_{up} is the annual maximum of 30 day moving averaged upstream runoff (m^3/s). For river channels where GWD-LR is not available, river channel width is determined by the empirical equation. The river channel height is determined by an empirical equation:

$$B = \max[0.14 \times R_{up}^{0.40}, 2.00] \tag{4}$$

where B is the river channel height (m) and R_{up} is the annual maximum of 30 day moving averaged upstream runoff (m^3/s).

In this study, runoff offline simulations by *Kim et al*. [2009] calculated from a land surface model, MATSIRO-GW, was used to force river routing in CaMa-Flood. MATSIRO, "the minimal advanced treatments of surface interaction and runoff" was developed by *Takata et al*. [2003] and represents energy and water exchange between atmosphere and land. MATSIRO has been updated to incorporate groundwater representation (MATSIRO-GW) [*Koirala et al*., 2014]. MATSIRO-GW driven by climate forcing JRA-25 [*Onogi et al*., 2007] was employed in this study.

CaMa-Flood has been validated in several previous studies. *Yamazaki et al*. [2011] demonstrated that modeled river discharges were in good agreement with observations in most of the major continental rivers of the world. A striking feature of CaMa-Flood is that it can delineate bifurcating river channels (i.e., river channels representing multiple downstream directions) and its scheme was found to achieve better simulations of flood inundation, particularly in low-lying deltaic regions such as the Mekong [*Yamazaki et al*., 2014a],

the GBM [*Ikeuchi et al*., 2015], and the Chao Phraya river basins [*Mateo et al*., 2017], compared to simulations without channel bifurcation.

In this study, we simulated discharge over the period 1979–2010 at a subdaily time step. The simulation domain is the whole world at a spatial resolution of 15 min (approximately 25 km at the equator) and for validation of the coupled model (section 3.2) the spatial resolution was set as 0.1° (approximately 10 km at the equator) over each river basin (the GBM and the Mekong). Inundation depth (i.e., water level above the top of a river channel) is downscaled onto an 18 arc sec (approximately 500 m at the equator) high-resolution DEM by comparing the elevation of pixels in the DEM against the water level modeled at a coarse resolution (15 arc min). Since CaMa-Flood incorporates the same high-resolution subgrid topography for both river routing and downscaling, the water volumes before and after downscaling are consistent. This downscaling method can produce inundation information detailed enough to assess fluvial flood risks (see further detail in the supporting information of *Ikeuchi et al*. [2015]).

2.2. Global Tide and Surge Reanalysis (GTSR) Data Set

GTSR is the world's first dynamically derived data set of global coastal water levels. To develop GTSR, *Muis et al*. [2016] used hydrodynamic modeling approach to obtain a reanalysis of tides and surges during the period of 1979–2014. These were further processed to obtain extreme sea levels for different return periods, by extracting annual maxima and fitting a Gumbel distribution. Recent studies such as *Vousdoukas et al*. [2017] used similar methods, but included estimates of extreme storm surges in Europe for future climate projections. *Cid et al*. [2017] used statistical methods to derive global surge levels by utilizing the 2 Dimensions Gravity Waves model (MOG2D) for the correction of altimetry data (the Dynamic Atmospheric Correction). While statistical methods might be more suitable for long-term projections than hydrodynamic methods in terms of computational loads, we employ the latter in the present study because our simulation period is the past 30 years, hence the predominance of hydrodynamic modeling in accuracy outweighs computational load. Furthermore, *Muis et al*. [2017] has shown that GTSR provides better estimates of extreme sea levels compared to a previous data set of global extreme sea levels (DINAS-COAST Extreme Sea Levels data set) that had been the only global data available for over a decade before the development of GTSR, so the use of GTSR in this study is appropriate for the present study.

In GTSR, surges and tides are separately calculated, based on two hydrodynamic models: Global Tide and Surge Model (GTSM) to model surge levels, and Finite Element Solution (FES2012) to calculate tidal levels. GTSM is forced by atmospheric pressure and wind speed derived from the ERA-Interim reanalysis data set [*Dee et al*., 2011]. GTSM uses the Delft3D Flexible Mesh software [*Kernkamp et al*., 2011]. Its striking advantage is the application of an unstructured grid, facilitating simulation at flexible resolutions depending on location (i.e., higher resolution in shallow continental shelf than offshore areas), which greatly reduces computational demands compared to traditional structured grids. Spatial resolutions vary from 0.5° (∼50 km at the equator) in deeper parts to 3 arc min (∼5 km at the equator) in shallow coasts. The bathymetry data for GTSM are derived from General Bathymetric Chart of the Oceans 2014 (GEBCO_2014) [*Weatherall et al*. 2015], which are interpolated onto the computational grid. Tides are simulated using the FES2012 hydrodynamic model [*Carrère et al*., 2012], which is a global tide model assimilating satellite altimetry data. Tides calculated by FES2012 are superimposed on the surge data of GTSM. The temporal resolution of the resulting GTSR data set is 10 min.

GTSR outputs are available for 16,611 locations, which agree with the centroids of the coastal segments from the Dynamic Interactive Vulnerability Assessment (DIVA) database, an integrated model for global coastal systems [*Hinkel and Klein*, 2009]. The selection of 16,611 stations ensures coverage of coastal areas around the world while still keeping the amount of data manageable. Modeled results were validated against sea level observations derived from the University of Hawaii Sea Level Center (UHSLC, http://uhslc.soest.hawaii.edu/data/download/fd). According to *Muis et al*. [2016], the root-mean-square error (RMSE) and the Pearson correlation coefficient of total sea levels for all 472 gauging stations around the world during the period 1980–2011 were 0.15 m and 0.83, respectively. The RMSE and the correlation coefficient averaged for 64 gauging stations in the Southeast and East Asia regions (0°N–40°N, 65°E–125°E) were 0.24 m and 0.87, respectively. These results show the GTSR performance to reasonably reproduce sea levels.

2.3. Improved Storm Surge Simulation Using IBTrACS for Specific Surge Events

Muis et al. [2016] noted that extreme sea levels caused by tropical storms in GTSR are underestimated because of the low spatial and temporal resolution of the ERA-Interim meteorological forcing. Hence, in the analysis of 2007 Cyclone Sidr, storm surge was calculated by forcing GTSM with the observed tropical storm track to enhance tropical storm simulation [*Verlaan et al*., 2016]. The observed tropical cyclone track was taken from the IBTrACS data set [*Knapp et al*., 2010]. Based on a number of tropical cyclone parameters, wind speed, and pressure fields are generated by applying the Wind Enhance Scheme (WES) software developed by Deltares (https://content.oss.deltares.nl/delft3d/manuals/Delft3D-WES_User_Manual.pdf), which follows the parametric hurricane model developed by *Holland* [1980]. Since the IBTrACS data set provides a global data set of best tracks of historical cyclones, the use of it can be considered a good approach to improve estimates of storm surge for global-scale analyses.

The time span of the storm surge data set is from 6:00 on 10 November to 18:00 on 15 November when Cyclone Sidr made its landfall on Bangladesh. While we did not use modeled surge results after 18:00 on 15 November due to the lack of cyclone track data of IBTrACS after its landfall, we assumed that the storm surge data before this time includes the maximum occurring water levels. To obtain sea level data after 18:00 on 15 November, the tidal component is extrapolated symmetrically. We assumed that this procedure would not make essential difference in analyzing the potential impact of storm surge on fluvial flooding, which is the main objective of this study.

2.4. Representation of Dynamic Sea Level Boundary Conditions in CaMa-Flood

To couple river and coast models, a scheme for expressing the effects of storm surge on river discharge calculations is required. The original version of CaMa-Flood assumed constant sea levels of 0 m relative to the SRTM vertical datum. While the effect of sea level variation is usually negligible in global simulations of river routing, its variation has a meaningful impact on river discharge in low-lying areas. Thus, in this study we developed a new scheme for CaMa-Flood to deal with dynamic sea levels at river mouths due to tides and storm surges. The newly developed scheme can be described as follows:

1. Reading sea level boundary conditions from gridded data at each calculation time step; and
2. Calculating hydraulics at the river mouth considering dynamic sea level.

We connect the nearest GTSR output to each river mouth in CaMa-Flood. To avoid connecting CaMa-Flood and GTSR points that are too far apart, we set a threshold the distance between a CaMa-Flood river grid cell and an allocated GTSR output location should be $<$50 km. Note that by following this method, some river mouth grid cells in CaMa-Flood are not connected to corresponding GTSR data when the distance is too large. In such a case, input sea levels in CaMa-Flood remain 0 m. Following this method, two-dimensional gridded data of sea level at river mouths were generated every 10 min from the GTSR data.

3. Results and Discussion

3.1. Coupling Simulation at a Global-Scale and Continental-Scale

Global river discharge simulations were conducted using CaMa-Flood with input of sea levels of GTSR. Figure 1 shows the difference in annual maximum water surface elevation between simulations with and without input sea levels (simulation results with GTSR minus those without GTSR). Although the absolute values of the differences are moderate ($<$0.1 m) in most regions of the world, we see that sea levels greatly influence simulation results in low-lying flat areas such as the Amazon basin and many river basins in Southeast and East Asia (i.e., increases in water level $>$0.5 m).

Focusing on Southeast and East Asia, six major rivers (catchment areas $>$160,000 km^2) are selected to analyze the impact of dynamic sea levels on fluvial flooding: the Indus, Ganges, Irrawaddy, Chao Phraya, Mekong, and Yangtze. Figure 2 shows input sea levels modeled with GTSR (top figures) and water surface elevation modeled with CaMa-Flood with (red line) and without (blue line) GTSR (bottom figures). Even in the Indus, Irrawaddy, Chao Phraya, and Mekong Rivers, the differences in water levels caused by dynamic sea levels can be up to 0.5 m. In the Ganges and Yangtze Rivers, the differences are even greater, namely more than 1 m, due to the high surge levels calculated by GTSR. For example, the peak water levels in the Ganges in 2006 are 1.32 m higher with the input of GTSR, and $\sim$1.33 higher in the Yangtze river in 2002. The reason for this is that input sea levels show $>$1 m amplitude variation, which may be caused by their

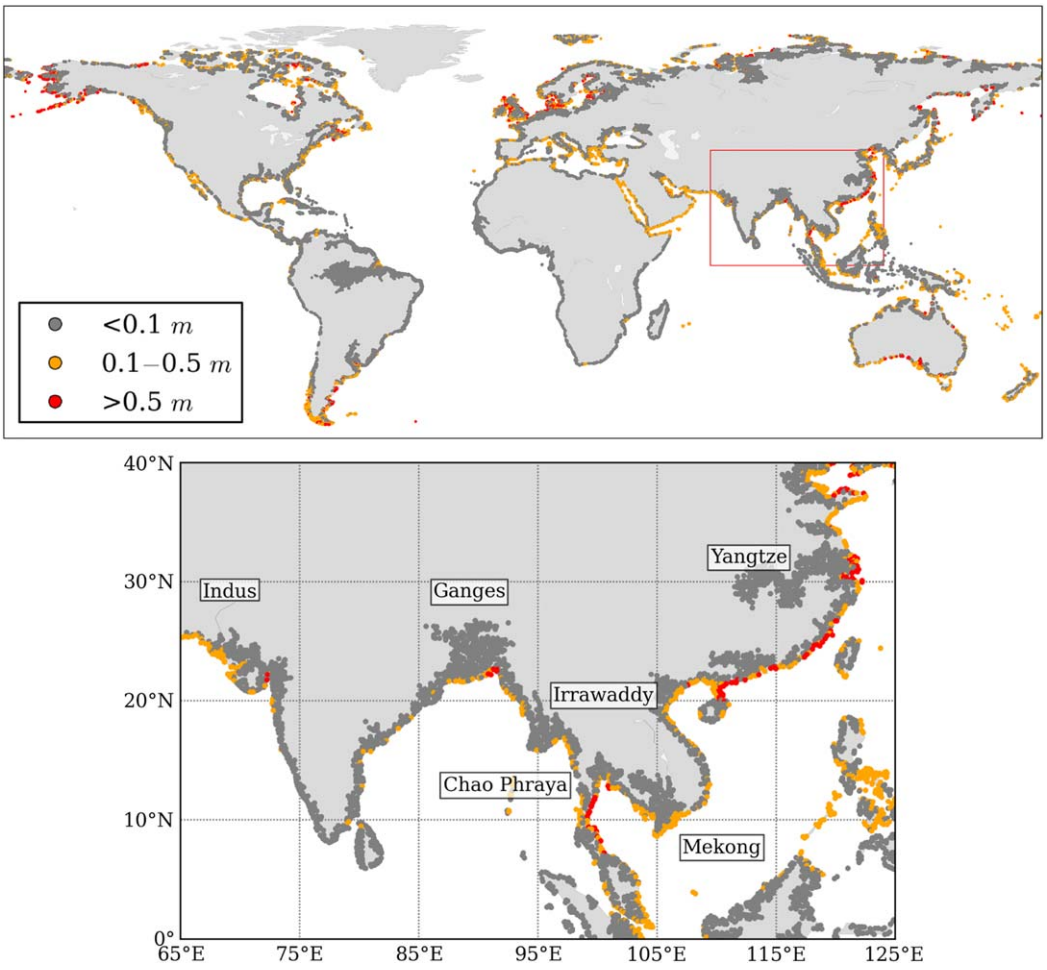

Figure 1. Difference in annual maxima of water surface elevation (m) for the year 2005 between simulations with and without GTSR at a global-scale (top figure) and a continental-scale (Asian region, bottom figure). The magnified domain shown in the bottom figure is indicated as a red rectangle in the top figure.

physical characteristics, such as the fact that they face open oceans and are surrounded by a narrow-shaped topography. Moreover, in the Chao Phraya River, the incorporation of GTSR strengthens the seasonal variation in river water level, i.e., increasing the high water level (+0.32 m) and decreasing the low water level (−0.40 m) due to the correspondence of seasonal patterns. In the Mekong River, similar impacts are seen but with a smaller extent (+0.20 m for increase in high water level and −0.17 m for decrease in low water level in case of 2003). Hence, the incorporation of the sea level reanalysis data set has a large effect on river water level variation.

3.2. Validation of Coupling GTSR and CaMa-Flood in the GBM Delta and the Mekong Delta

Modeled results of river water levels obtained by CaMa-Flood coupled with GTSR are validated against observations obtained in the GBM Delta (Figures 3a and 3b), and in the Mekong Delta (Figures 3c and 3d). The gauging stations (CD: Chandpur, DL: Daulakhan, and RY: Rayenda for the GBM Delta, and CT: Can Tho, MTo: My Tho, and MTu: My Thuan for the Mekong Delta) are located in the coastal region in the delta as shown in Figures 3a and 3c. By incorporating the tide and surge reanalysis data set, the reproducibility of water surface elevations was enhanced. For example, correlation coefficients were slightly increased for all gauging points, and in the case of the GBM basins, RMSE and relative errors were reduced (Table 1). Furthermore, for all gauging stations in the GBM Delta, water levels become significantly larger by inclusion of GTSR in river discharge simulations: maxima of increases in modeled water levels are 0.97 m at CD, 1.19 m at DL, and 0.48 m at RY. Note that there are missing values in observations (shown as gaps in gray lines in Figure 3b); these coefficients were calculated over the period for which observed data are available.

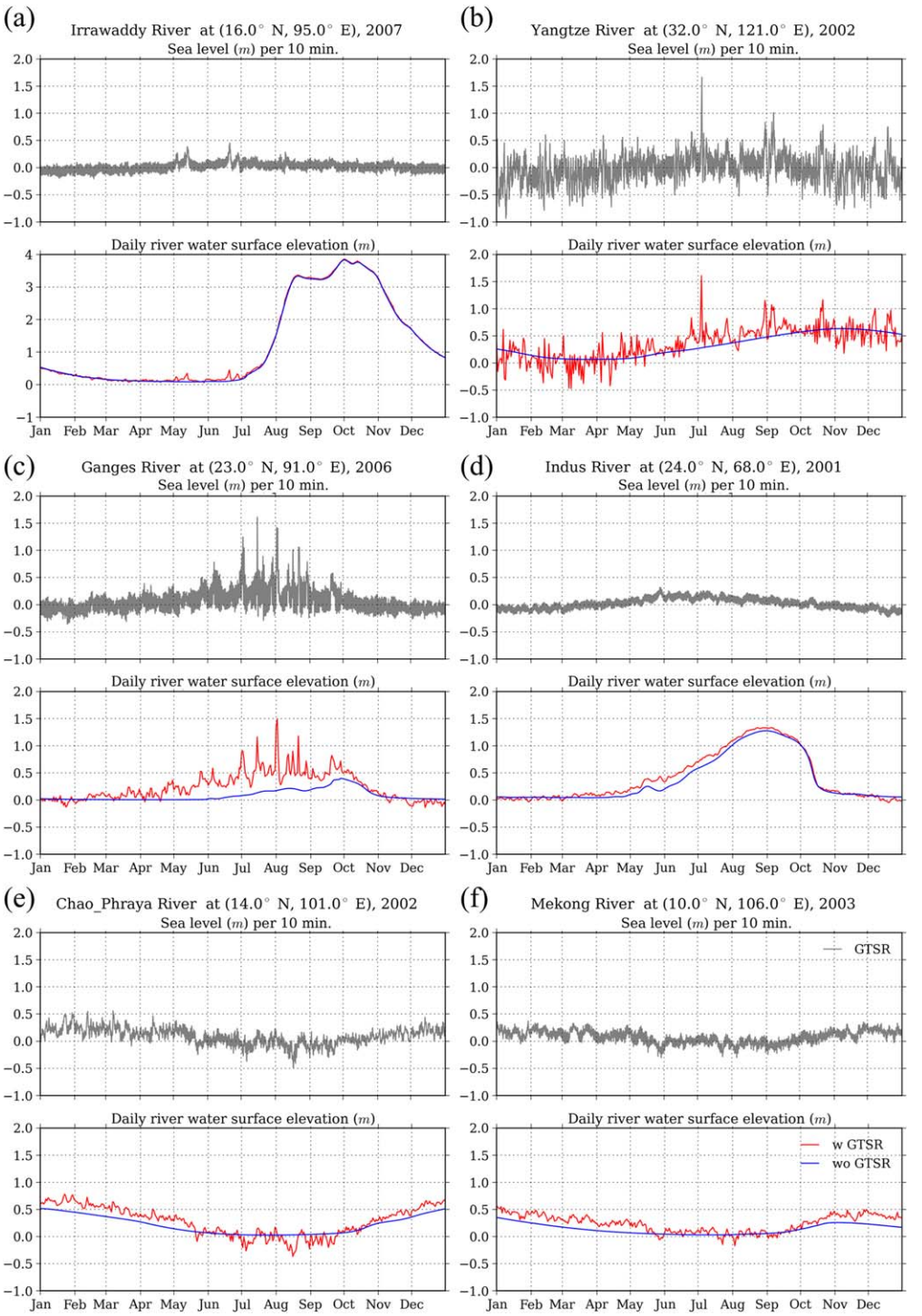

Figure 2. Input water levels (m) per 10 min at river mouths (gray lines in upper parts) and water surface elevation (m) modeled by CaMa-Flood with and without GTSR (red and blue lines in lower parts) in six Asian rivers: (a) Irrawaddy River, (b) Yangtze River, (c) Ganges River, (d) Indus River, (e) Chao Phraya River, and (f) Mekong River. Each plot shows water levels in different years, which are indicated in the respective titles.

While the coupling of GTSR and CaMa-Flood results in an increase in the correlation coefficients for water level simulations, their impacts are seemingly small. This is because water levels at river mouths of large-scale rivers are predominantly determined by upstream river discharges, making the effects of tide and surge relatively small. In addition, simulated water levels are underestimated at the station DL, and do not

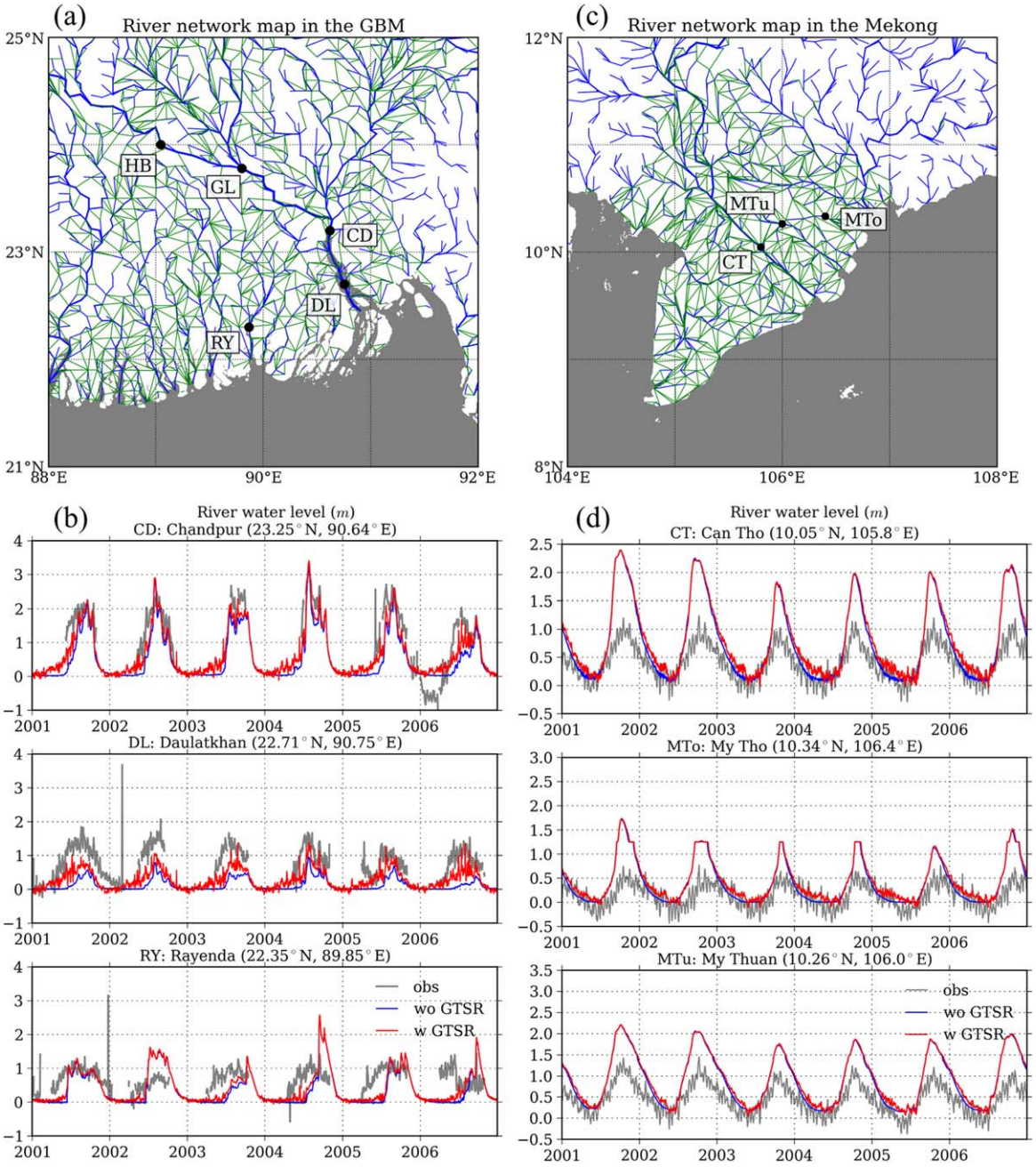

Figure 3. (a) The river network map in CaMa-Flood and gauging stations (CD, DL, and RY) used for validation in the GBM Delta. Blue and green lines indicate main river channels and bifurcation river channels, respectively. Names and locations for each station are denoted in Figure 3b. Two other stations (HB and GL) are indicated in Figure 7. (b) Validation of water levels (m) simulated by the CaMa-Flood coupled with GTSR at three stations in the GBM Delta. Gray, blue, and red lines indicate observations, CaMa-Flood simulations without GTSR, and with GTSR, respectively. Gaps in gray lines indicate missing values. (c) Same as Figure 3a but for the Mekong Delta. (d) Same as Figure 3b but for the Mekong Delta.

match well with observations at RY. This may be due to the errors in determining river channel cross-sectional parameters (river channel width and height). As discussed in section 2.1, the river channel width is defined by GWD-LR or the empirical equation. In this case, river channel width values at CD and DL are obtained from GWD-LR, but not at RY. In the coastal region of the GBM Delta, river channel width of GWD-LR tends to be large compared to inland regions, probably because that region is composed of both river inflow and seawater intrusion, making it difficult to exactly define the river channel width. In addition, the river channel height is determined only by the empirical equation. The use of these empirical equations may also be one cause for the mismatch between simulations and observations, such as at RY. Another potential source of the error at RY may be the existence of seasonal cycles of sea surface height driven by

Table 1. Correlation Coefficients, Root-Mean-Square Errors (RMSEs), and Relative Errors

River	Station	w/wo GTSR	Correlation Coefficient	RMSE (m)	Relative Error (%)
GBM	CD	wo	0.712	0.670	29.9
		w	0.723	0.511	15.0
	DL	wo	0.554	0.762	77.7
		w	0.614	0.545	51.1
	RY	wo	0.232	0.619	32.9
		w	0.261	0.559	21.8
Mekong	CT	wo	0.889	0.551	−83.9
		w	0.890	0.580	−99.2
	MTo	wo	0.697	0.411	−174
		w	0.748	0.426	−211
	MTu	wo	0.908	0.538	−91.1
		w	0.914	0.560	−99.6

Kelvin waves in the Bay of Bengal, which can reach about 0.5 m [*Rao et al.*, 2010], and by a strong modulation in the amplitude of the semi-diurnal lunar tide, which is of order 10 cm [*Tazkia et al.*, 2017], which processes are not represented in GTSR. The current modeling framework does not include such a complex physical phenomenon unique to the Bay of Bengal. Finally, modeled river water levels in the Mekong Delta are overestimated compared to observations, shown as relatively large RMSEs and relative errors in Table 1. The reason for the overall overestimation of river water levels in CaMa-Flood is because bathymetric depths of bifurcating river channels are relatively low, resulting in decreases in outgoing water flow from main river channels and hence increases in water levels in main river channels. Channel bathymetric depths are currently one of the largest uncertainties in river hydrodynamic modeling, though some efforts to improve them are ongoing [e.g., *Durand et al.*, 2008; *Yoon et al.*, 2012]. While these limitations exist, the increase in correlation coefficients of river water levels due to the incorporation of coastal water level data indicates that the coupling scheme developed in this study has the ability to achieve more reasonable flood simulations than without the coupling.

3.3. Simulation of the Impact of Cyclone Sidr on Fluvial Flooding

Before carrying out the coupled river-coast flood simulations, we checked the performance of the modeled sea levels of GTSM for Cyclone Sidr in the GBM Delta by comparing it with observed water levels obtained by BIWTA (Bangladesh Inland Water Transport Authority). Note that these data are not from GTSR, but are the results obtained from GTSM driven by the observed storm tracks as explained in section 2.3. Figure 4a shows the observed and modeled water levels at two locations (Khepupara and Hiron Point). When we compare the locations of GTSM outputs (the black stars in Figure 4b) and observation points (the blue and red dots in Figure 4b), it can be seen that there are no GTSM outputs near Khepupara. On the other hand, one GTSM output is very closely located near Hiron Point, so the modeled water levels at this point are depicted in Figure 4a.

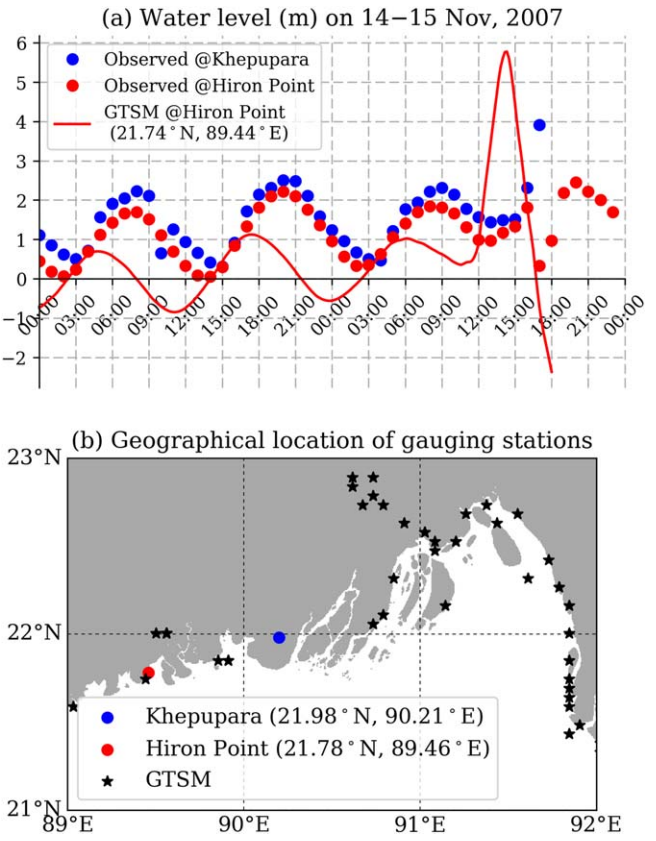

Figure 4. (a) Validation of GTSM (the red line) against observed water levels (the blue and red dots) during 14–15 November, 2007. (b) Locations of GTSM outputs (black stars) and observation stations (the blue and red dots).

Comparing the modeled and observed water levels in Figure 4a, we can see that the tidal period and amplitude are similar (approximately 12 h and 1.6 m) but the timing and the absolute values are different between them (discrepancies of around 2 h and 0.8 m). As *Krien et al.* [2017] indicated, there can be a difference in the timing of cyclone landfall between observed water level data and cyclone track data (Joint

Table 2. Validation of Peak Water Levels During the Cyclone Event

	Latitude (°N)	Longitude (°E)	Maximum Storm Surge (m)
JSCE (2008)	22.23	89.83	6.47
IWM (2009)	22.30	89.85	5.00
GTSM	22.01	89.56	5.61

Typhoon Warning Center, JTWC in their case). In our case, we used the cyclone track from IBTrACS, and the comparison results show that there appears to be a lag in the timing of landfall. In addition, although we subtracted mean sea levels (MSS_CNES_CLS2011, available on http://www.aviso.altimetry.fr/en/data/products/auxiliary-products/mss.html) from the observed water levels, there are still discrepancies between observations and simulations, which may originate from the relatively coarse model resolution, potential biases in representation of the nearshore bathymetry as well as an inadequate parametrization of bottom friction in the Bay of Bengal.

Regarding the storm surge heights caused by Cyclone Sidr, the modeled storm surges were much higher than the observed ones at Hiron Point as shown in Figure 4a. The reason for this overestimation may be the biases in the bathymetry of GEBCO. *Krien et al*. [2016] demonstrated (Figure 3 in their paper) that the submarine regions are too shallow in GEBCO (around 2–4 m), which may make the storm surge height too large in some regions. Other sources of the overestimation may be the problems listed in the previous paragraph and a location difference between the tide gauge and model output stations (e.g., the output point is closer to the ocean in the model than the actual location of Hiron Point). Potential errors in observed water levels can be another reason for the discrepancy. Observed water levels at Khepupara show an increase toward 18:00 on 15 November, however it is reported that the tide gauge stopped working suddenly after that [*Krien et al*., 2017], so that there may be a possibility that the observations may not capture actual maxima of peak water levels in this event.

In order to analyze the ability of GTSM to reproduce peak water levels, we referred to two previous studies that provide storm surge height data [*Japan Society of Civil Engineers* (*JSCE*), 2008; *Institute of Water Modelling* (*IWM*), 2009], which were introduced in *Lewis et al.* [2013]. Table 2 shows the validation results of peak water levels during the cyclone event. The output location of GTSM is selected such that its distance from the location of observed data is the minimum. This result indicates that the peak height of the modeled sea level (5.61 m) agrees with the reported extreme sea level caused by Cyclone Sidr, which ranges from 5.00 to 6.47 m.

Simulations of flood inundation using CaMa-Flood with the input of the storm surge caused by Cyclone Sidr were conducted. Figures 5 and 6 show the spatial distribution of modeled inundation depths with (hereafter called Surge experiment) and without (NoSurge experiment) surge input, as well as the difference between the two simulations (i.e., results of Surge experiment minus results of NoSurge experiment). Figure 7 shows a time series of inundation depths at four gauging stations. In Figure 7, the solid and dotted lines indicate modeled results of Surge and NoSurge experiments, respectively. The temporal resolution of both results is 10 min, although the results of the NoSurge experiments show gradual variation in inundation depths compared to the Surge experiments, because the original temporal resolution of input runoff calculated by MATSIRO is daily. The inundation depth at the river mouth starts to increase by $>$2 m at around 14:00 in the Padma River (the downstream flow from a confluence of the Ganges and the Brahmaputra Rivers). About 4 h later (18:00), inundation depth at the river mouth reaches its peak ($>$3 m). After that, the inundation depth in the Padma River starts to decrease, whereas the upstream rivers (the Ganges and the Brahmaputra Rivers) still show increasing inundation depths. An increase of about 0.7 m in water level can be seen at a location more than 200 km from the river mouth (GL in Figure 7). Note that observations are not available during this period (15–16 November 2007), so we could not validate the modeled inundation depth.

The propagation of storm surge through rivers is clearly represented in Figures 5 and 6. If we do not include input sea levels, the modeled inundation depths remain low (shown as the dotted lines in Figure 7). This indicates that the incorporation of a storm surge reanalysis data set has a substantial impact on fluvial flood simulations during storm surge events. Furthermore, the propagation effect is expressed by the backwater effect, which has been found to be critical in fluvial flood simulations with sea level rise [*Ikeuchi et al*., 2015]. Hence, this study not only supports that finding, but also adds new insights, such as revealing spatiotemporal characteristics of flood inundation in the case of cyclone-induced storm surges.

3.4. Limitations

This study has several limitations related to the use of CaMa-Flood, GTSR, and the coupling scheme, which are discussed in this subsection. While CaMa-Flood can simulate river channel bifurcation flows, water flow

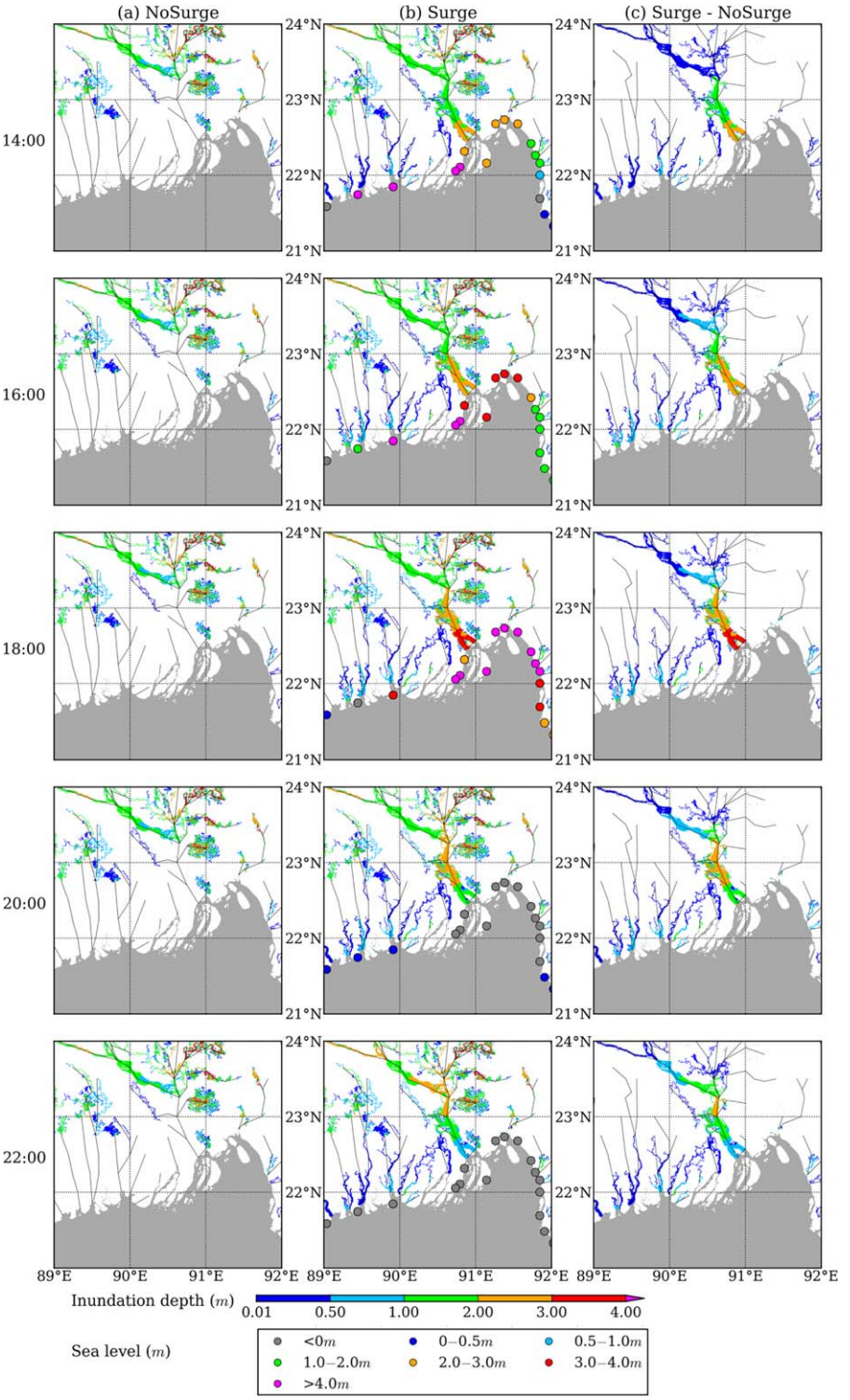

Figure 5. (a) Inundation depth (m) in the simulations without input sea levels (NoSurge), (b) with input sea levels (Surge), and (c) the differences between them (Surge-NoSurge) on 15 November at 2 h intervals. Dots in Figure 5b indicate the input sea levels along the coast.

via small channels such as artificial canals cannot be modeled due to the difficulty in classifying them as bifurcating river channels [*Yamazaki et al.*, 2014a]. This may lead to an underestimation when representing the impact of storm surge, such as surge wave propagation through navigation channels [*Ebersole et al.*,

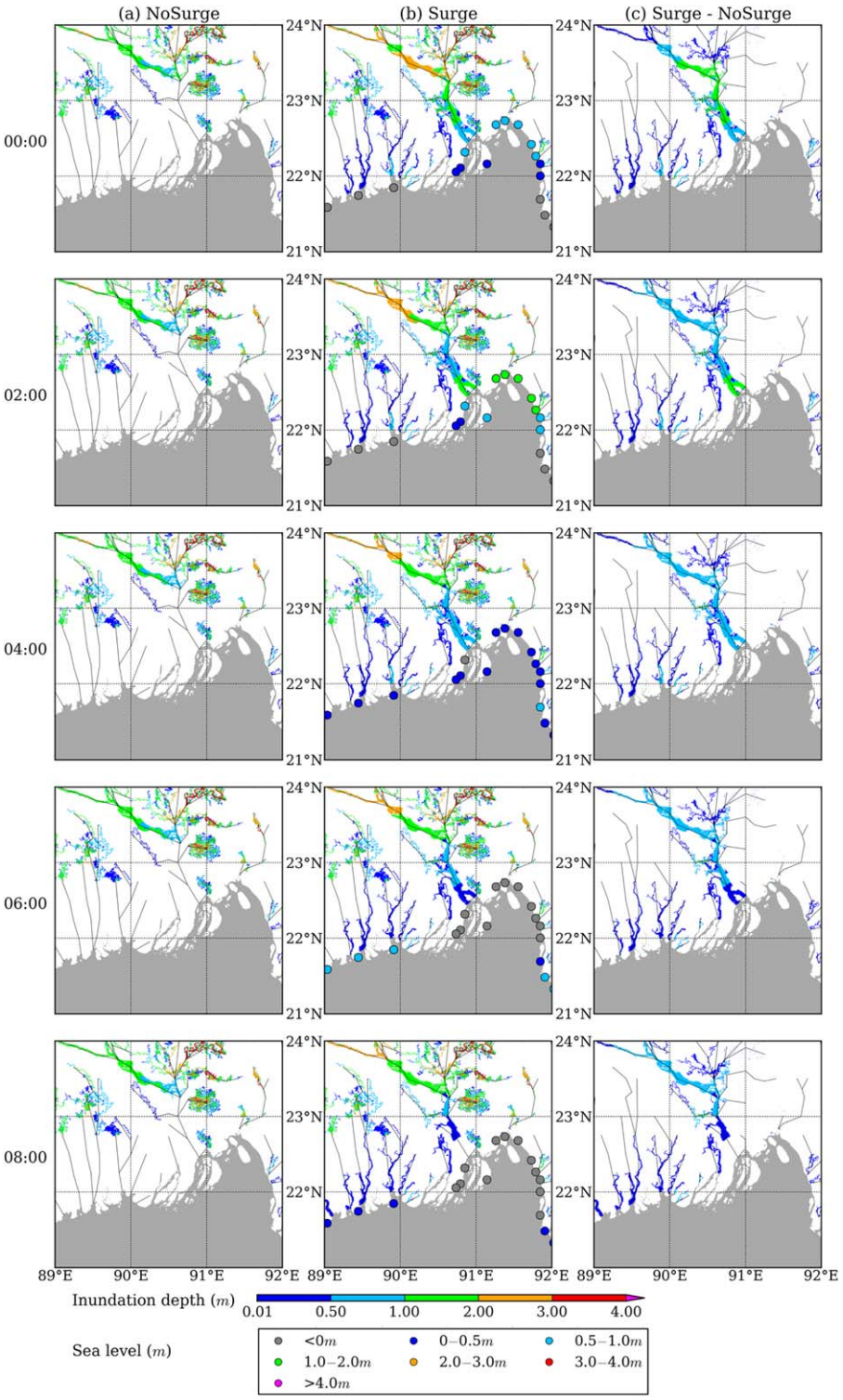

Figure 6. Same as Figure 5 but on 16 November.

2010]. As discussed in section 3.2, the river channel height is estimated by an empirical equation, which can be a factor leading to over/underestimation.

Second, the current version of GTSR does not deal with baroclinic effects (i.e., pressure gradients due to differences in water density) and nonlinear interaction between tides and surges [*Muis et al.*, 2016]. Other

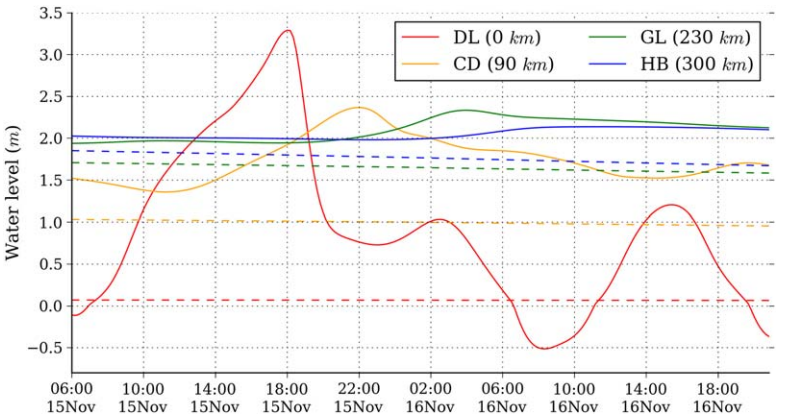

Figure 7. Modeled river water levels (m) at four gauging stations during Cyclone Sidr's landfall. Solid and dotted lines denote simulation results with and without storm surge input, respectively. Geographical locations of gauging stations are shown in Figure 3a. Numbers in brackets in the legend are the distances from the river mouth to each point.

wave effects, such as wave setup induced by wave radiation stress [*Bunya et al*., 2010] and/or contribution of short waves to regulate surface stresses [*Bertin et al*., 2015] should be addressed. In particular, nonlinear tide-surge interaction can cause significant increase in sea levels [e.g., approximately 0.2 m in Canada, *Bernier and Thompson*, 2007], 0.5 m in UK [*Horsburgh and Wilson*, 2007], and 1.0 m in the Bay of Bengal [*Krien et al*., 2017]. These can be contributors to determine sea levels along coasts, so the total water levels of the tide and surge reanalysis used in this study may be biased particularly in regions where tide-surge interactions are significant. In addition, although GEBCO, the data used as the global bathymetry in GTSM, is widely used in studies of coastal hydrodynamics, it was shown to contain significant errors in the Bay of Bengal (e.g., too much shallow bathymetry in submarine regions), compared to a newly and locally developed bathymetry data set obtained by extensively utilizing nautical charts and river survey results available in that region [*Krien et al*., 2016]. This kind of the state-of-the-art bathymetric data should be employed in further studies that specifically address coastal hydrodynamics in the Bay of Bengal [e.g., *Krien et al*., 2017].

Finally, the current model coupling scheme includes neither pluvial flooding nor coastal flooding. This is because of the lack of a modeling scheme for them in global river routing models. While this study focused on the impact of storm surges on rivers, the inverse effect was not taken into account; freshwater input to the ocean may also be a factor affecting sea levels. Despite these limitations, the coupling methods proposed in this paper can contribute to improving our simulation of water levels in delta regions affected by both river flooding and surge. The coupling also serves as a starting point for further improvements in the modeling of these compound floods at large-scales to global-scales.

4. Conclusions

In this study, we focused on the impact of storm surges on fluvial flooding in mega-delta regions, within a framework of global flood modeling. A global river routing model was modified to handle the dynamically changing sea levels at river mouths. Each river mouth grid cell in the river model was connected with the nearest output from the tide and surge model. Moreover, we successfully conducted coupled simulations of the global river routing model with the global tide and surge data set, showing a large influence on modeled water levels particularly in deltas and estuaries. This scheme was applied to one specific cyclone event, Cyclone Sidr in the GBM Delta in 2007, as a case study. The cyclonic storm surge caused a $>$3 m increase in inundation depth at the river mouth, along with a 0.7 m increase at a point approximately 200 km away from the river mouth. Including the sea level dynamics in global river routing models has been shown to improve the performance of the river model and have a large effect on the inundation estimates. Future work stemming from this study includes the development of holistic representations of flooding in coastal regions, which could be achieved by representing coastal flooding induced by storm surges.

Acknowledgments
This paper was financially supported by the Funding Program for the Global Environmental Research Fund (S-10 and S-14) by the Ministry of the Environment, Japan; the Program for Risk Information on Climate Change by the Ministry of Education, Culture, Sports, Science, and Technology (MEXT), Japan; JSPS KAKENHI grants 16J07523, 16H06291. PJW received funding from the Netherlands Organisation for Scientific Research through VIDI grant 016.161.324. We thank Shinichiro Kida in Kyushu University, Japan, for his invaluable comments. We are grateful to A. K. M. Saiful Islam in Institute of Water and Flood Management, Bangladesh University of Engineering and Technology, Bangladesh, for providing us with the observed water level data by BIWTA during Cyclone Sidr as part of research collaboration. The CaMa-Flood model is available on the developer's webpage (http://hydro.iis.u-tokyo.ac.jp/~yamadai/cama-flood/), the 1-in-100-year extreme sea levels of the GTSR data set are freely available online at the archive of the 4TU.Research Data (https://data.4tu.nl/repository/uuid:aa4a6ad5-e92c-468e-841b-de07f7133786) and other parts of the GTSR data set may be available upon request to the developer (sanne.muis@vu.nl). Simulation results presented in this work may be available upon request to the corresponding author (ikeuchi@rainbow.iis.u-tokyo.ac.jp).

References

Androulidakis, Y. S., K. D. Kombiadou, C. V. Makris, V. N. Baltikas, and Y. N. Krestenitis (2015), Storm surges in the Mediterranean Sea: Variability and trends under future climatic conditions, *Dyn. Atmos. Oceans*, *71*, 56–82, doi:10.1016/j.dynatmoce.2015.06.001.

Bates, P. D., M. S. Horritt, and T. J. Fewtrell (2010), A simple inertial formulation of the shallow water equations for efficient two-dimensional flood inundation modelling, *J. Hydrol.*, *387*(1), 33–45, doi:10.1016/j.jhydrol.2010.03.027.

Bernier, N. B., and K. R. Thompson (2007), Tide-surge interaction off the east coast of Canada and northeastern United States, *J. Geophys. Res.*, *112*, C06008, doi:10.1029/2006JC003793.

Bertin, X., K. Li, A. Roland, and J. R. Bidlot (2015), The contribution of short-waves in storm surges: Two case studies in the Bay of Biscay, *Cont. Shelf Res.*, *96*, 1–15, doi:10.1016/j.csr.2015.01.005.

Bunya, S., et al. (2010), A high-resolution coupled riverine flow, tide, wind, wind wave, and storm surge model for southern Louisiana and Mississippi. Part I: Model development and validation, *Mon. Weather Rev.*, *138*(2), 345–377, doi:10.1175/2009MWR2906.1.

Carrère, L., F. Lyard, M. Cancet, A. Guillot, and L. Roblou (2012), FES2012: A new global tidal model taking advantage of nearly 20 years of altimetry measurements, in *Proceedings of the 20 Years of Altimetry*, Venice, Italy, 2012.

Chen, W.-B., and W.-C. Liu (2014), Modeling flood inundation induced by river flow and storm surges over a river basin, *Water*, *6*(10), 3182–3199, doi:10.3390/w6103182.

Chow, V. T. (1959), *Open-Channel Hydraulics*, 680 pp., McGraw-Hill, New York.

Cid, A., P. Camus, S. Castanedo, F. J. Méndez, and R. Medina (2017), Global reconstructed daily surge levels from the 20th century reanalysis (1871–2010), *Global Planet. Change*, *148*, 9–21, doi:10.1016/j.gloplacha.2016.11.006.

Cisneros, J. B. E., T. Oki, N. W. Arnell, G. Benito, J. G. Cogley, P. Döll, T. Jiang, and S. S. Mwakalila (2014), Freshwater resources, in *Climate Change 2014: Impacts, Adaptation, and Vulnerability, Part A: Global and Sectoral Aspects, Contribution of Working Group II to the Fifth Assessment Report of the Intergovernmental Panel on Climate Change*, edited by C. B. Field et al., pp. 229–269, Cambridge Univ. Press, Cambridge, U. K.

Dankers, R., et al. (2014), First look at changes in flood hazard in the Inter-Sectoral Impact Model Intercomparison Project ensemble, *Proc. Natl. Acad. Sci. U. S. A.*, *111*(9), 3257–3261, doi:10.1073/pnas.1302078110.

Dee, D. P., et al. (2011), The ERA-Interim reanalysis: Configuration and performance of the data assimilation system, *Q. J. R. Meteorol. Soc.*, *137*(656), 553–597, doi:10.1002/qj.828.

Durand, M., K. M. Andreadis, D. E. Alsdorf, D. P. Lettenmaier, D. Moller, and M. Wilson (2008), Estimation of bathymetric depth and slope from data assimilation of swath altimetry into a hydrodynamic model, *Geophys. Res. Lett.*, *35*, L20401, doi:10.1029/2008GL034150.

Ebersole, B. A., J. J. Westerink, S. Bunya, J. C. Dietrich, and M. A. Cialone (2010), Development of storm surge which led to flooding in St. Bernard Polder during Hurricane Katrina, *Ocean Eng.*, *37*(1), 91–103, doi:10.1016/j.oceaneng.2009.08.013.

Farr, T. G., et al. (2007), The shuttle radar topography mission, *Rev. Geophys.*, *45*, RG2004, doi:10.1029/2005RG000183.

Hallegatte, S., C. Green, R. J. Nicholls, and J. Corfee-Morlot (2013), Future flood losses in major coastal cities, *Nat. Clim. Change*, *3*(9), 802–806, doi:10.1038/NCLIMATE1979.

Hinkel, J., and R. J. T. Klein (2009), Integrating knowledge to assess coastal vulnerability to sea-level rise: The development of the DIVA tool, *Global Environ. Change*, *19*(3), 384–395, doi:10.1016/j.gloenvcha.2009.03.002.

Hinkel, J., D. Lincke, A. T. Vafeidis, M. Perrette, R. J. Nicholls, R. S. J. Tol, B. Marzeion, X. Fettweis, C. Ionescu, and A. Levermann (2014), Coastal flood damage and adaptation costs under 21st century sea-level rise, *Proc. Natl. Acad. Sci. U. S. A.*, *111*(9), 3292–3297, doi:10.1073/pnas.1222469111.

Hirabayashi, Y., S. Kanae, S. Emori, T. Oki, and M. Kimoto (2008), Global projections of changing risks of floods and droughts in a changing climate, *Hydrol. Sci. J.*, *53*(4), 754–772, doi:10.1623/hysj.53.4.754.

Hirabayashi, Y., R. Mahendran, S. Koirala, L. Konoshima, D. Yamazaki, S. Watanabe, H. Kim, and S. Kanae (2013), Global flood risk under climate change, *Nat. Clim. Change*, *3*(9), 816–821, doi:10.1038/NCLIMATE1911.

Hoitink, A. J. F., and D. A. Jay (2016), Tidal river dynamics: Implications for deltas, *Rev. Geophys.*, *54*, 240–272, doi:10.1002/2015RG000507.

Holland, G. J. (1980), An analytic model of the wind and pressure profiles in hurricanes, *Mon. Weather Rev.*, *108*(8), 1212–1218, doi:10.1175/1520-0493(1980)108 < 1212:AAMOTW>2.0.CO;2.

Horsburgh, K. J., and C. Wilson (2007), Tide-surge interaction and its role in the distribution of surge residuals in the North Sea, *J. Geophys. Res.*, *112*, C08003, doi:10.1029/2006JC004033.

Ikeuchi, H., Y. Hirabayashi, D. Yamazaki, M. Kiguchi, S. Koirala, T. Nagano, A. Kotera, and S. Kanae (2015), Modeling complex flow dynamics of fluvial floods exacerbated by sea level rise in the Ganges-Brahmaputra-Meghna Delta, *Environ. Res. Lett.*, *10*(12), 124011, doi:10.1088/1748-9326/10/12/124011.

Institute of Water Modelling (IWM) (2009), Use existing data on available digital elevation models to prepare useable tsunami and storm surge inundation risk maps for the entire coastal region, final report vol. I: Tsunami and strom surge inundation of the coastal area of Bangladesh', Inst. of Water Modell., Bangladesh. [Available at http://kmp.dmic.org.bd/bitstream/handle/123456789/88/52.%20Tsunami%20and%20Strom%20Surge%20Inundation.pdf?sequence=1, last accessed on 24 Sept. 2016.]

Japan Society of Civil Engineers (JSCE) (2008), Investigation Report on the Storm Surge Disaster by Cyclone SIDR in 2007, Bangladesh. [Available at http://www.jsce.or.jp/report/46/files/Bangladesh_Investigation.pdf, last accesses on 24 Sept. 2016.]

Jongman, B., P. J. Ward, and J. C. J. H. Aerts (2012a), Global exposure to river and coastal flooding: Long term trends and changes, *Global Environ. Change*, *22*(4), 823–835, doi:10.1016/j.gloenvcha.2012.07.004.

Jongman, B., H. Kreibich, H. Apel, J. I. Barredo, P. D. Bates, L. Feyen, A. Gericke, J. Neal, J. Aerts, and P. J. Ward (2012b), Comparative flood damage model assessment: Towards a European approach, *Nat. Hazards Earth Syst. Sci.*, *12*(12), 3733–3752, doi:10.5194/nhess-12-3733-2012.

Karim, M. F., and N. Mimura (2008), Impacts of climate change and sea-level rise on cyclonic storm surge floods in Bangladesh, *Global Environ. Chang.*, *18*(3), 490–500, doi:10.1016/j.gloenvcha.2008.05.002.

Kernkamp, H. W. J., A. Van Dam, G. S. Stelling, and E. D. de Goede (2011), Efficient scheme for the shallow water equations on unstructured grids with application to the Continental Shelf, *Ocean Dyn.*, *61*(8), 1175–1188, doi:10.1007/s10236-011-0423-6.

Kew, S. F., F. M. Selten, G. Lenderink, and W. Hazeleger (2013), The simultaneous occurrence of surge and discharge extremes for the Rhine delta, *Nat. Hazards Earth Syst. Sci.*, *13*(8), 2017–2029, doi:10.5194/nhess-13-2017-2013.

Kim, H., P. Yeh, T. Oki, and S. Kanae (2009), Role of rivers in the seasonal variations of terrestrial water storage over global basins, Geophys. *Res. Lett.*, *36*, L17402, doi:10.1029/2009GL039006.

Klerk, W. J., H. C. Winsemius, W. J. van Verseveld, A. M. R. Bakker, and F. L. M. Diermanse (2015), The co-incidence of storm surges and extreme discharges within the Rhine–Meuse Delta, *Environ. Res. Lett.*, *10*(3), 035005, doi:10.1088/1748-9326/10/3/035005.

Knapp, K. R., M. C. Kruk, D. H. Levinson, H. J. Diamond, and C. J. Neumann (2010), The international best track archive for climate stewardship (IBTrACS), *Bull. Am. Meteorol. Soc.*, *91*(3), 363–376, doi:10.1175/2009BAMS2755.1.

Koirala, S., P. J. F. Yeh, Y. Hirabayashi, S. Kanae, and T. Oki (2014), Global-scale land surface hydrologic modeling with the representation of water table dynamics, *J. Geophys. Res. Atmos.*, *119*, 75–89, doi:10.1002/2013JD020398.

Krien, Y., et al. (2016), Improved bathymetric dataset and tidal model for the Northern Bay of Bengal, *Mar. Geod.*, *39*(6), 422–38, doi:10.1080/01490419.2016.1227405.

Krien, Y., et al. (2017), Towards improved storm surge models in the Northern Bay of Bengal, *Cont. Shelf Res.*, *135*, 58–73, doi:10.1016/j.csr.2017.01.014.

Lehner, B., K. Verdin, and A. Jarvis (2008), New global hydrography derived from spaceborne elevation data, *Eos*, *89*(10), 93–94, doi:10.1029/eost2008EO10.

Leonard, M., S. Westra, A. Phatak, M. Lambert, B. Van den Hurk, K. McInnes, J. Risbey, S. Schuster, D. Jakob, and M. Stafford-Smith (2014), A compound event framework for understanding extreme impacts, *WIREs Clim. Change*, *5*, 113–128, doi:10.1002/wcc.252.

Lewis, M., P. Bates, K. Horsburgh, J. Neal, and G. Schumann (2013), A storm surge inundation model of the northern Bay of Bengal using publicly available data, *Q. J. R. Meteorol. Soc.*, *139*, 358–369, doi:10.1002/qj.2040.

Lin, N., and K. Emanuel (2016), Grey swan tropical cyclones, *Nat. Clim. Change*, *6*(1), 106–111, doi:10.1038/NCLIMATE2777.

Mateo, C. M. R., D. Yamazaki, H. Kim, A. Champathong, J. Vaze, and T. Oki (2017), Impacts of spatial resolution and representation of flow connectivity on large-scale simulation of floods, *Hydrol. Earth Syst. Sci. Discuss.*, doi:10.5194/hess-2016-620, in review. [Available at https://www.hydrol-earth-syst-sci-discuss.net/hess-2016-620/.]

Milly, P. C. D., R. T. Wetherald, K. A. Dunne, and T. L. Delworth (2002), Increasing risk of great floods in a changing climate, *Nature*, *415*(6871), 514–517, doi:10.1038/415514a.

Muis, S., M. Verlaan, H. C. Winsemius, J. C. J. H. Aerts, and P. J. Ward (2016), A global reanalysis of storm surges and extreme sea levels, *Nat. Commun.*, *7*, 11969, doi:10.1038/ncomms11969.

Muis, S., M. Verlaan, R. J. Nicholls, S. Brown, J. Hinkel, D. Lincke, A. T. Vafeidis, P. Scussolini, H. C. Winsemius, and P. J. Ward (2017), A comparison of two global datasets of extreme sea levels and resulting flood exposure, *Earth's Future*, *5*, 379–392, doi:10.1002/2016EF000430.

Onogi, K., et al. (2007), The JRA-25 reanalysis, *J. Meteorol. Soc. Jpn.*, *85*(3), 369–432, doi:10.2151/jmsj.85.369.

Rao, R. R., M. S. Girish Kumar, M. Ravichandran, A. R. Rao, V. V. Gopalakrishna, and P. Thadathil (2010), Interannual variability of Kelvin wave propagation in the wave guides of the equatorial Indian Ocean, the coastal Bay of Bengal and the southeastern Arabian Sea during 1993–2006, *Deep Sea Res., Part I*, *57*(1), 1–13, doi:10.1016/j.dsr.2009.10.008.

Seneviratne, S. I., et al. (2012), Changes in climate extremes and their impacts on the natural physical environment, in *Managing the Risks of Extreme Events and Disasters to Advance Climate Change Adaptation*, edited by C. Field et al., Cambridge Univ. Press, Cambridge, U. K.

Skinner, C. J., T. J. Coulthard, D. R. Parsons, J. A. Ramirez, L. Mullen, and S. Manson (2015), Simulating tidal and storm surge hydraulics with a simple 2D inertia based model, in the Humber Estuary, UK, *Estuarine Coastal Shelf Sci.*, *155*, 126–136, doi:10.1016/j.ecss.2015.01.019.

Syvitski, J. P. M., and Y. Saito (2007), Morphodynamics of deltas under the influence of humans, *Global Planet. Change*, *57*(3–4), 261–282, doi:10.1016/j.gloplacha.2006.12.001.

Syvitski, J. P. M., et al. (2009), Sinking deltas due to human activities, *Nat. Geosci.*, *2*(10), 681–686, doi:10.1038/NGEO629.

Takata, K., S. Emori, and T. Watanabe (2003), Development of the minimal advanced treatments of surface interaction and runoff, *Glob. Planet. Change*, *38*, 209–222, doi:10.1016/S0921-8181(03)00030-4.

Tazkia, A. R., Y. Krien, F. Durand, L. Testut, A. K. M. S. Islam, F. Papa, and X. Bertin (2017), Seasonal Modulation of M2 Tide in the Northern Bay of Bengal, *Cont. Shelf Res.*, *137*, 154–62, doi:10.1016/j.csr.2016.12.008.

Trigg, M. A., et al. (2016), The credibility challenge for global fluvial flood risk analysis, *Environ. Res. Lett.*, *11*(9), 94014, doi:10.1088/1748-9326/11/9/094014.

Van Der Knijff, J. M., J. Younis, and A. P. J. De Roo (2010), LISFLOOD: A GIS-based distributed model for river basin scale water balance and flood simulation, *Int. J. Geogr. Inf. Sci.*, *24*(2), 189–212, doi:10.1080/13658810802549154.

Verlaan, M., H. Winsemius, D. Vatvani, S. Muis, and P. Ward (2016), Tropical storm tracks in a global tide and storm surge reanalysis, *EGU General Assembly 2016*, Vienna, Austria.

Vousdoukas, M. I., E. Voukouvalas, A. Annunziato, A. Giardino, and L. Feyen (2016), Projections of extreme storm surge levels along Europe, *Clim. Dyn.*, *47*, 3171–3190, doi:10.1007/s00382-016-3019-5.

Vousdoukas, M. I., L. Mentaschi, E. Voukouvalas, M. Verlaan, and L. Feyen (2017), Extreme sea levels on the rise along Europe's coasts, *Earth's Future*, *5*, 304–323, doi:10.1002/2016EF000505.

Wahl, T., S. Jain, J. Bender, S. D. Meyers, and M. E. Luther (2015), Increasing risk of compound flooding from storm surge and rainfall for major US cities, *Nat. Clim. Change*, *5*(12), 1093–1097, doi:10.1038/NCLIMATE2736.

Ward, P. J., B. Jongman, F. S. Weiland, A. Bouwman, R. van Beek, M. F. P. Bierkens, W. Ligtvoet, and H. C. Winsemius (2013), Assessing flood risk at the global scale: Model setup, results, and sensitivity, *Environ. Res. Lett.*, *8*(4), 044019, doi:10.1088/1748-9326/8/4/044019.

Ward, P. J., B. Jongman, M. Kummu, M. D. Dettinger, F. C. S. Weiland, and H. C. Winsemius (2014), Strong influence of El Niño Southern Oscillation on flood risk around the world, *Proc. Natl. Acad. Sci. U. S. A.*, *111*(44), 15659–15664, doi:10.1073/pnas.1409822111.

Ward, P. J., et al. (2015), Usefulness and limitations of global flood risk models, *Nat. Clim. Change*, *5*, 712–715, doi:10.1038/nclimate2742.

Weatherall, P., K. M. Marks, M. Jakobsson, T. Schmitt, S. Tani, J. E. Arndt, M. Rovere, D. Chayes, V. Ferrini, and R. Wigley (2015), A new digital bathymetric model of the world's oceans, *Earth Space Sci.*, *2*, 331–345, doi:10.1002/2015EA000107.

Winsemius, H. C., L. P. H. Van Beek, B. Jongman, P. J. Ward, and A. Bouwman (2013), A framework for global river flood risk assessments, *Hydrol. Earth Syst. Sc.*, *17*(5), 1871–1892, doi:10.5194/hess-17-1871-2013.

Winsemius, H. C., et al. (2016), Global drivers of future river flood risk, *Nat. Clim. Change*, *6*, 381–385, doi:10.1038/nclimate2893.

Wong, P. P., I. J. Losada, J.-P. Gattuso, J. Hinkel, A. Khattabi, K. L. McInnes, Y. Saito, and A. Sallenger (2014), Coastal systems and low-lying areas, in *Climate Change 2014: Impacts, Adaptation, and Vulnerability, Part A: Global and Sectoral Aspects, Contribution of Working Group II to the Fifth Assessment Report of the Intergovernmental Panel on Climate Change*, edited by C. B. Field et al., pp. 361–409, Cambridge Univ. Press, Cambridge, U. K.

Yamazaki, D., T. Oki, and S. Kanae (2009), Deriving a global river network map and its sub-grid topographic characteristics from a fine-resolution flow direction map, *Hydrol. Earth Syst. Sci.*, *13*(11), 2241–2251, doi:10.5194/hess-13-2241-2009.

Yamazaki, D., S. Kanae, H. Kim, and T. Oki (2011), A physically based description of floodplain inundation dynamics in a global river routing model, *Water Resour. Res.*, *47*, W04501, doi:10.1029/2010WR009726.

Yamazaki, D., G. A. M. de Almeida, and P. D. Bates (2013), Improving computational efficiency in global river models by implementing the local inertial flow equation and a vector-based river network map, *Water Resour. Res.*, *49*, 7221–7235, doi:10.1002/wrcr.20552.

Yamazaki, D., T. Sato, S. Kanae, Y. Hirabayashi, and P. D. Bates (2014a), Regional flood dynamics in a bifurcating mega delta simulated in a global river model, *Geophys. Res. Lett.*, *41*, 3127–3135, doi:10.1002/2014GL059744.

Yamazaki, D., F. O'Loughlin, M. A. Trigg, Z. F. Miller, T. M. Pavelsky, and P. D. Bates (2014b), Development of the global width database for large rivers, *Water Resour. Res.*, *50*, 3467–3480, doi:10.1002/2013WR014664.

Yoon, Y., M. Durand, C. J. Merry, E. A. Clark, K. M. Andreadis, and D. E. Alsdorf (2012), Estimating river bathymetry from data assimilation of synthetic SWOT measurements, *J. Hydrol.*, *464*, 363–375, doi:10.1016/j.jhydrol.2012.07.028.